N94-23664

THREE-DIMENSIONAL SOLIDIFICATION AND MELTING USING MAGNETIC FIELD CONTROL

George S. Dulikravich* and Vineet Ahuja**
Department of Aerospace Engineering
The Pennsylvania State University, University Park, PA 16802, USA

ABSTRACT

A new two-fluid mathematical model for fully three-dimensional steady solidification under the influence of an arbitrary acceleration vector and with or without an arbitrary externally applied steady magnetic field have been formulated and integrated numerically. The model includes Joule heating and allows for separate temperature-dependent physical properties within the melt and the solid. Latent heat of phase change during melting/solidification was incorporated using an enthalpy method. Mushy region was automatically captured by varying viscosity orders of magnitude between liquidus and solidus temperature. Computational results were obtained for silicon melt solidification in a parallelepiped container cooled from above and from a side. The results confirm that the magnetic field has a profound influence on the solidifying melt flow field thus changing convective heat transfer through the boundaries and the amount and shape of the solid accrued. This suggests that development of a quick-response algorithm for active control of three-dimensional solidification is feasible since it would require low strength magnetic fields.

INTRODUCTION

Possible means of devising controlling mechanisms for solidification and bulk single crystal growth from a melt is of practical importance to many industrial processes [Kosovic, Dulikravich and Lee 1991; Dulikravich, Kosovic and Lee 1992]. We will demonstrate the quantified effects of a fully three-dimensional solidification control using magnetic fields. If there are no electric charges in the melt and no external electric field is applied, a magnetohydrodynamic (MHD) model [Stuetzer 1962] can be applied. MHD flows without solidification have already been numerically analyzed in three-dimensions [Ozoe and Okada 1989; Lee and Dulikravich 1991]. It was only recently that various researchers have demonstrated numerically the effects of the magnetic field in two-dimensional [Salcudean and Sabhapathy 1990; Dulikravich, Kosovic and Lee 1991; Kosovic and Dulikravich 1991] and in three-dimensional [Dulikravich, Ahuja and Lee 1993a, 1993b; Dulikravich and Ahuja 1993] solidification.

Our objective is to use a single system of governing equations in the entire domain which could consist of the melt, mixture of the melt and the solid (mushy region), or the solid alone. In other words, we want to use a single system of partial differential equations that treats both the melt and the solid as liquids, while allowing each of the two liquids to have its own set of temperature-dependent physical properties (density, heat capacity, thermal conductivity, electric permitivity, thermal expansion, magnetic permeability, etc.). A crucial difference between the two liquids is that the liquid which models the solid phase ($T < T_{solidus}$) must be assigned extremely high viscosity. Hence, velocities interior to the regions occupied by the liquid that models the solid phase will be practically zero. Consequently, we will refer to this artificially extremely viscous liquid as "solid", while the pure melt ($T > T_{liquidus}$) will be called "liquid".

---

* Associate Professor.

** Graduate Research Assistant.

Mass fraction of the liquid at any point in the domain determines locally to what extent should physical properties of the liquid or the solid be taken into account. Since latent heat released or absorbed per unit mass of the mushy region is proportional to the local volumetric fraction, f, occupied by the liquid in a particular computational cell, this ratio is often modeled [Voller and Swaminathan 1991] as

$$f = \frac{V_{liquid}}{V_{liquid} + V_{solid}} = \left(\frac{\theta - \theta_{solidus}}{\theta_{liquidus} - \theta_{solidus}}\right)^n \qquad (1)$$

where the exponent "n" is typically $0.2 < n < 5$. Here, the non-dimensional temperature is defined as $\theta = (T - T_0)/\Delta T_0$ where T is the temperature measured in degrees. Typically, either $\Delta T_0 = T_{liquidus} - T_{solidus}$ and $T_0 = T_{solidus}$ or $\Delta T_0 = T_{hot} - T_{cold}$ and $T_0 = T_{cold}$. The latent heat, L, is released in the mushy region (where $T_{liquidus} > T > T_{solidus}$) in proportion to the fraction f of the liquid in the mixture. Liquid density, ρ_l is assumed to vary linearly as a function of non-dimensional temperature

$$\rho_l' = 1 + \left.\frac{\partial(\rho_l/\rho_{0l})}{\partial\theta}\right|_0 (\theta - \theta_0) = 1 - \alpha^*_{0l}(\theta - \theta_0) \qquad (2)$$

with a similar expression for the solid phase. We will use subscripts "l" and "s" to designate liquid and solid phase, respectively. If subscript "o" designates reference values, then the non-dimensionalization can be performed as follows

$$v^* = \frac{v}{|v_0|} \qquad g^* = \frac{g}{|g_0|} \qquad H^* = \frac{H}{|H_0|} \qquad x^* = \frac{x}{l_0} \qquad t^* = \frac{t\,|v_0|}{l_0} \qquad p^* = \frac{p}{\rho_0\,|v_0|^2} \qquad (3)$$

$$\rho_l^* = \frac{\rho_{0l}}{\rho_0}\rho_l' \qquad \mu_l^* = \frac{\mu_{0l}}{\mu_0}\mu_l' \qquad k_l^* = \frac{k_{0l}}{k_0}k_l' \qquad c_l^* = \frac{c_{0l}}{c_0}c_l' \qquad \alpha_l^* = \frac{\alpha_{0l}}{\alpha_0}\alpha_l' \qquad (4)$$

with similar expressions for the solid phase. Here, **v**, **g**, **H** and **x** are vectors of velocity, gravity acceleration, magnetic field and spatial position vector, respectively. Similarly, μ, k, c and α are coefficients of viscosity, heat conductivity, heat capacity and thermal expansion, respectively. Hydrodynamic pressure, coefficients of electric conductivity and magnetic permeability are designated with p, σ and γ, respectively. In this work we assumed that σ and γ do not vary with temperature ($\sigma_l^* = \sigma_{0l}/\sigma_0$, $\sigma_s^* = \sigma_{0s}/\sigma_0$, $\gamma_l^* = \gamma_{0l}/\gamma_0$ and $\gamma_s^* = \gamma_{0s}/\gamma_0$). Since the reference values designated with the subscript "o" are arbitrary, the non-dimensional numbers can be defined as

$$Re = \frac{\rho_0\, v_0\, l_0}{\mu_0} \qquad Fr^2 = \frac{|v_0|^2}{|g_0|\, l_0} \qquad Ec = \frac{|v_0|^2}{c_0\,\Delta T_0} \qquad (5)$$

$$Pr = \frac{\mu_0\, c_0}{k_0} \qquad S_{te} = \frac{c_0\,\Delta T_0}{L_0} \qquad P_m = \frac{\gamma_0\,\sigma_0\,\mu_0}{\rho_0} \qquad (6)$$

$$Gr = \frac{\rho_o^2 \alpha_o |g_o| \Delta T_o l_o^3}{\mu_o^2} \qquad H_t = \gamma_o |H_o| l_o \left(\frac{\sigma_o}{\mu_o}\right)^{1/2} \tag{7}$$

Then, adopting an extended Boussinesq approximation [Gray and Giorgini 1976] to MHD flows, the non-dimensional Navier-Stokes equations for phase-changing mixtures of two liquids [Dulikravich and Ahuja 1993] become:
Mass conservation for two-phase MHD flows

$$\nabla^* \cdot v^* = 0 \tag{8}$$

Linear momentum conservation for two-phase MHD flows with thermal buoyancy and magnetic force

$$\bar{\bar{\rho}} \frac{\partial v^*}{\partial t^*} + f \rho_l^* \nabla^* \cdot (v^* v^* + \bar{\bar{p}}_l^* I) + (1-f) \rho_s^* \nabla^* \cdot (v^* v^* + \bar{\bar{p}}_s^* I)$$

$$= f [\nabla^* \cdot (\frac{\mu_l^*}{Re} (\nabla^* v^* + (\nabla^* v^*)^T)) + \rho_l^* (\gamma_l^* \frac{H_t^2}{P_m Re^2} (\nabla^* \times H^*) \times H^* + \alpha_l^* \frac{Gr\theta}{Re^2} g^*)]$$

$$+(1-f)[\nabla^* \cdot (\frac{\mu_s^*}{Re} (\nabla^* v^* + (\nabla^* v^*)^T)) + \rho_s^* (\gamma_s^* \frac{H_t^2}{P_m Re^2} (\nabla^* \times H^*) \times H^* + \alpha_s^* \frac{Gr\theta}{Re^2} g^*)] \tag{9}$$

Energy conservation for incompressible two-phase MHD flows including Joule heating

$$(f \rho_l^* (c_{el}^* \theta)_{,\theta} + (1-f) \rho_s^* (c_{es}^* \theta)_{,\theta}) \frac{\partial \theta}{\partial t^*} + f \rho_l^* \nabla^* \cdot (c_{el}^* \theta v^*) + (1-f) \rho_s^* \nabla^* \cdot (c_{es}^* \theta v^*)$$

$$= f (\frac{1}{RePr} \nabla^* \cdot (k_l^* \nabla^* \theta) + \frac{\gamma_l^*}{\sigma_l^*} \frac{H_t^2 Ec}{P_m^2 Re^3} (\nabla^* \times H^*) \cdot (\nabla^* \times H^*))$$

$$+ (1-f) (\frac{1}{RePr} \nabla^* \cdot (k_s^* \nabla^* \theta) + \frac{\gamma_s^*}{\sigma_s^*} \frac{H_t^2 Ec}{P_m^2 Re^3} (\nabla^* \times H^*) \cdot (\nabla^* \times H^*)) \tag{10}$$

Magnetic field transport equations for two-phase MHD flows

$$\frac{\partial H^*}{\partial t^*} - \nabla^* \times (v^* \times H^*) = \frac{f/(\sigma_l^* \gamma_l^*) + (1 - f)/(\sigma_s^* \gamma_s^*)}{P_m R_e \bar{\bar{\rho}}} \nabla^{*2} H^* \tag{11}$$

Here, $\bar{\bar{\rho}} = f \rho_l^* + (1 - f) \rho_s^*$, where $f = 1$ for $\theta > \theta_{liquidus}$ and $f = 0$ for $\theta < \theta_{solidus}$. Non-dimensional hydrostatic, hydrodynamic, and magnetic pressures were combined to give

$$\bar{p}_l^* = \frac{p^*}{\rho_l^*} + \frac{\phi^*}{Fr^2} + \frac{\gamma_l^* H_t^2}{P_m Re^2} H^* \cdot H^* \qquad \bar{p}_s^* = \frac{p^*}{\rho_s^*} + \frac{\phi^*}{Fr^2} + \frac{\gamma_s^* H_t^2}{P_m Re^2} H^* \cdot H^* \tag{12}$$

where ϕ^* is the non-dimensional gravity potential defined as $g^* = \nabla^* \phi^*$. We used an enthalpy method to formulate the equivalent specific heat coefficients in the liquid and the solid phases are $c_{el}^* = c_l^* - \frac{1}{S_{te}} \frac{\partial f}{\partial \theta}$ and $c_{es}^* = c_s^* - \frac{1}{S_{te}} \frac{\partial f}{\partial \theta}$, respectively. This expression allows latent heat to be released in the mushy region according to the empirical law given in equation (1).

At the solid walls, the velocity components were set to zero and the wall pressure was determined from the normal momentum equation. Wall temperatures were either specified or obtained from the specified wall heat fluxes and the points on the first grid layer off the walls. Magnetic field was either specified as uniform on a particular wall, or its normal derivative to the wall was set to zero. The governing system of eight partial differential equations (8-11) was transformed into a non-orthogonal curvilinear coordinate system compatible with a typical three-dimensional boundary-conforming structured computational grid. In such a way, the resulting finite difference algorithm for an iterative integration of the system can be applied to relatively arbitrary three-dimensional configurations. Since the system is singular (its time-dependent term in the mass conservation equation is zero), it can be integrated simultaneously only after introducing an artificially time-dependent term [Chorin 1967] in the mass conservation. Consequently, such an "artificial compressibility" iterative process does not follow physical time, but rather an artificial time coordinate. As a result, intermediate solutions are not time-accurate pictures of the flow field, but the final converged steady solution is accurate since the artificial compressibility term variation with iterations then becomes zero.

We are using an explicit four-step time-integration and central differencing in space. Since the magnetic field transport equations (11) are strongly parabolic (for the given velocity field), their allowable integration time step is much smaller than in the case of the Navier-Stokes equations (7-10). Consequently, we coded the three magnetic transport equations separately from the three-dimensional Navier-Stokes equations [Lee and Dulikravich 1991] so that we can use different time steps for the two systems. Communication between the two systems based on periodically updating source terms (thermal buoyancy and magnetic effect s) in the Navier-Stokes system.

NUMERICAL RESULTS

Based on this analytical model for a two-fluid MHD solidification, a fully three-dimensional MHD flow analysis computer program was developed. Numerical results from this code were compared with known three-dimensional MHD analytical solutions in the case of no heat transfer [Lee and Dulikravich 1991] and in the case of heat transfer but without solidification [Ozoe and Okada 1991]. In both cases the code proved to be highly accurate [Dulikravich, Ahuja and Lee 1993a]. This code was then augmented to incorporate temperature-dependent physical properties of the melt and the solid phase and the effects of latent heat release with an adequate account of the mushy region.

We decided to study the three-dimensional MHD effects on solidification by numerically analyzing an MHD solidification in a parallelepipedal closed container initially filled with molten silicon. The container was discretized with $40 \times 20 \times 20$ grid cells that were clustered symmetrically towards all the walls (Figure 1). Gravity was assumed to act vertically downward in the positive z-direction. If not indicated otherwise, the solid walls were thermally insulated. The values of the reference parameters were: $|v_o| = 0.02342$ m s^{-1}, $l_o = 0.02$ m, $|g_o| = 9.81$ m s^{-2}. Physical properties for silicon were compiled from a number of references (Table 1) which lead to

the following values of the non-dimensional numbers: Gr = 2.89 x 10^6, Re = $Gr^{1/2}$ = 1702, Ec = 2.589 x 10^{-8}, Pr = 0.01161, Pr = 4.255 x 10^{-6} and Ht = 837.3 Bo, where Bo is measured in Teslas. The exponent used in the model for latent heat release (1) was n = 5. Test cases were run with Ht = 0, 20, 30, 60 corresponding to the magnetic fields having strengths of 0 Tesla, 0.02389 Tesla, 0.03583 Tesla and 0.07166 Tesla, respectively.

Solidification From the Top

In this case the container had dimensions 0.04 m x 0.02 m x 0.02 m. Top wall was uniformly cooled below freezing temperature (θ = - 0.5) and the bottom wall was uniformly heated (θ = 0.5). A solidification case was first run without the magnetic field (Ht = 0). The computed contours of equal vertical velocity magnitude evaluated in the z^* = 0.3 horizontal plane (Fig. 2a) indicate strong upward melt motion mainly along the short vertical walls and a centrally located downward jet. This is more evident in Figures 2b (evaluated at y^* = 0.5 vertical mid-plane) and 2c (evaluated at x^* = 0.5 vertical mid-plane) where it is clear that almost one-third (4926 solidified cells out of 16000 computational cells in the container) solidified starting from the top wall [Kerr et al. 1990]. Evidently, heat transfer is carried out by both conduction and convection. The computed isotherms in the vertical y^* = 0.5 mid-plane (Fig. 2d) and in the vertical x^* = 0.5 mid-plane (Fig. 2e) indicate that the solid/melt interface is somewhat pulled down in the central part of the container due to the strong centrally located downward melt jet. After reaching the bottom of the container, the jet spreads out and starts mowing upwards along the side walls thus forming a deformed vertical thoroidal melt motion.

A uniform steady magnetic field of Ht = 20 was then assigned in the vertically downward direction (same as the gravity direction). The computed contours of equal vertical velocity magnitude evaluated in the z^* = 0.25 horizontal plane (Fig. 3a) now indicate that the peak upward melt motion is mainly along the long vertical walls, while the centrally located downward jet became narrower and developed a non-parabolic profile. It is especially important to notice that the velocity profiles close to the walls and the solid/melt interface became steeper (Fig. 3b and 3c) which is typical of MHD flows. This in turn caused enhanced heat convection in the mushy region resulting in less accrued solid (4773 solidified computational cells). Because of the stronger downward centrally located jet the computed isotherms in the vertical mid-planes indicate slight sagging of the solid/melt interface (Fig. 3d and 3e).

Finally, a uniform steady magnetic field of Ht = 60 was assigned in the vertically downward direction. The computed contours of equal vertical velocity magnitude evaluated in the z^* = 0.25 horizontal plane (Fig. 4a) indicate a dramatic change as compared to the two previous cases. Specifically, the peak upward melt motion is contained in a narrow region along the short vertical walls, while the centrally located downward jet became wider and developed a strongly double-parabolic profile (Fig. 4a). The magnitudes of velocity vector components in the entire flow field were substantially reduced (Fig. 4b and 4c) to about 30% of those in the case with Ht = 20. Because of the weaker and less concentrated downward centrally located jet the computed isotherms in the vertical mid-planes indicate that the solid/melt interface is more planar (Fig. 4d and 4e). In this case there were 4676 solidified computational cells.

Solidification From a Side

The solidification was then tested for the case where one vertical wall (x^* = 0) was kept uniformly hot (θ = 0.5) and the opposite vertical wall (x^* = 1) was at a uniformly below freezing temperature (θ = - 0.5). Three runs were performed; one without the magnetic field (Ht = 0) and the other two with a uniform external magnetic field (Ht = 30) applied in the vertical z-direction and horizontal x-direction, respectively. The container size in this case was 0.01 m x 0.01 m x 0.02 m.

In the case of no magnetic field (Ht = 0), the computed contours of equal z-momentum evaluated in the $z^* = 0.5$ horizontal mid-plane indicate (Fig. 5a) a single large vortex that rises the melt at the hot wall and descends it at the solid/melt interface (Fig. 5b). The computed isotherms in the vertical $y^* = 0.5$ (Fig. 5c) and $x^* = 0.5$ (Fig. 5d) mid-planes show that the solid/melt interface is highly curved and three-dimensional. In this case there were 3990 solidified computational cells.

When the uniform magnetic field of Ht = 30 was applied downward, the computed contours of equal z-momentum evaluated in the $z^* = 0.5$ horizontal mid-plane indicate (Fig. 6a) that the intensity of the single large vortex decreased (Fig. 6b). Also, a recirculation mini-vortex that existed at the lower corner of the hot vertical wall in the case without a magnetic field (Fig. 5b) was now eliminated. Computed isotherms in the vertical mid-planes (Fig. 6c and 6d) indicate that the solid/melt surface in this case became essentially two-dimensional. The number of solidified computational cells in this case increased significantly to 4283.

A uniform magnetic field of Ht = 30 was then applied horizontally in the hot-to-cold x-direction. The computed contours of equal z-momentum evaluated in the $z^* = 0.5$ horizontal mid-plane indicate (Fig. 7a) that the intensity of the single large vortex decreased even further (Fig. 7b). Computed isotherms in the vertical mid-planes (Fig. 7c and 7d) indicate that the solid/melt interface became essentially two-dimensional. The number of solidified computational cells in this case increased significantly to 4311.

REFERENCES

Chorin, A.: A Numerical Method for Solving Incompressible Viscous Flow Problems, Journal of Computational Physics. vol. 2, 1967, pp. 12-26.

Dulikravich, G.S., Ahuja, V. and Lee, S.: Three-Dimensional Solidification With Magnetic Fields and Reduced Gravity. AIAA paper 93-0912, Aerospace Sciences Meeting, Reno, Nevada, January 11-14, 1993a.

Dulikravich, G.S., Ahuja, V. and Lee, S.: Three-Dimensional Control of Crystal Growth Using Magnetic Fields, SPIE paper 1916-07, Proceedings of Smart Structures and Materials Conference, Albuquerque, N. M., February 1-4, 1993b.

Dulikravich, G.S. and Ahuja, V.: Modeling Three-Dimensional Solidification With Magnetic Fields and Reduced Gravity. To appear in Internat. J. of Heat and Mass Transfer, 1993.

Dulikravich, G.S., Kosovic, B. and Lee, S.: Solidification in Reduced Gravity With Magnetic Fields and Temperature-Dependent Physical Properties, Symposium on Heat and Mass Transfer in Solidification Processing, Editors: S.G. Advani and C. Beckermann, ASME WAM'91, Atlanta, GA, Dec. 1-6, 1991, ASME HTD-Vol. 175/MD-Vol.25, 1991, pp. 61-73,

Dulikravich, G.S., Kosovic, B. and Lee, S.: Magnetized Fiber Orientation Control in Solidifying Composites: Numerical Simulation, 28th ASME National Heat Transfer Conference, San Diego, CA., August 9-12, 1992, Symposium on Transport Phenomena in Materials Processing and Manufacturing, Editors: M. Charmchi et al., ASME HTD-Vol. 196, 1992, pp. 135-144; also in Journal of Heat Transfer. vol.115, 1993, pp. 255-262.

Gray, D.D. and Giorgini, A.: The Validity of the Boussinesq Approximation for Liquids and Gases, International Journal of Heat and Mass Transfer, vol. 19, 1976, pp. 545-551.

Kerr,R.C., Woods, A.W., Worster, M.G. and Huppert, H.E.: Solidification of an Alloy Cooled From Above. Part 1. Equilibrium Growth. Journal of Fluid Mechanics, vol. 216, 1990, pp. 323-342.

Kosovic, B., Dulikravich, G.S. and Lee, S.: Freezing Under the Influence of a Magnetic Field: Computer Simulation, Proceedings of ICHMT International Symposium on Macroscopic and Microscopic Heat & Mass Transfer in Biomedical Engineering, Editors: K.Diller and A. Shitzer, Athens, Greece, Sept. 2-6, 1991, Elsevier Press, 1992, pp. 307-326.

Lee, S. and Dulikravich, G.S.: Magnetohydrodynamic Steady Flow Computations in Three Dimensions, Internat. Journal for Numerical Methods in Fluids. vol. 13, No. 8, 1991, pp. 917-936.

Ozoe, H. and Okada, K.: The Effect of the Direction of the External Magnetic Field on the Three-Dimensional Natural Convection in a Cubical Enclosure, International Journal of Heat and Mass Transfer. vol. 32, No. 2, 1989, pp. 1939-1954.

Poirier, D. and Salcudean, M.: On Numerical Methods Used in Mathematical Modeling of Phase Change in Liquid Metals. ASME paper 86-WAM/HT-22, Anaheim, CA, Dec. 7-12, 1986.

Salcudean, M. and Sabhapathy, P.: Numerical Study of Liquid Encapsulated Czochralski Growth of Gallium Arsenide With and Without an Axial Magnetic Field, ASME MD-Vol. 20, Symposium on Computer Modeling and Simulation of Manufacturing Processes, Editors: Singh, B., Im,Y. T., Haque, I. and Altan, C., Book No. G00552, 1990, pp. 115-127.

Stuetzer, O.M.: Magnetohydrodynamics and Electrohydrodynamics, The Physics of Fluids. vol. 5, No. 5 , 534-544 (1962).

Voller, V.R. and Swaminathan, C.R.: General Source-Based Method for Solidification Phase Change. Numerical Heat Transfer, Part B. vol. 19, 1991, pp. 175-189.

ρ_l [kg m^{-3}]	2550
ρ_s [kg m^{-3}]	2330
c_l [J kg^{-1} K^{-1}]	1059
c_s [J kg^{-1} K^{-1}]	1038
k_l [W m^{-1} K^{-1}]	64
k_s [W m^{-1} K^{-1}]	22
T_l [K]	1685
T_m [K]	1683
T_s [K]	1681
μ [kg m^{-1} s^{-1}]	7.018 x 10^{-4}
α_l [K^{-1}]	1.41 x 10^{-4}
α_s [K^{-1}]	1.41 x 10^{-4}
L [J kg^{-1}]	1803000
σ_l [W^{-1} m^{-1}]	12.3 x 10^5
σ_s [W^{-1} m^{-1}]	4.3 x 10^4
γ [Tm A^{-1}]	4π x 10^{-6}

Table 1. Physical properties used for silicon.

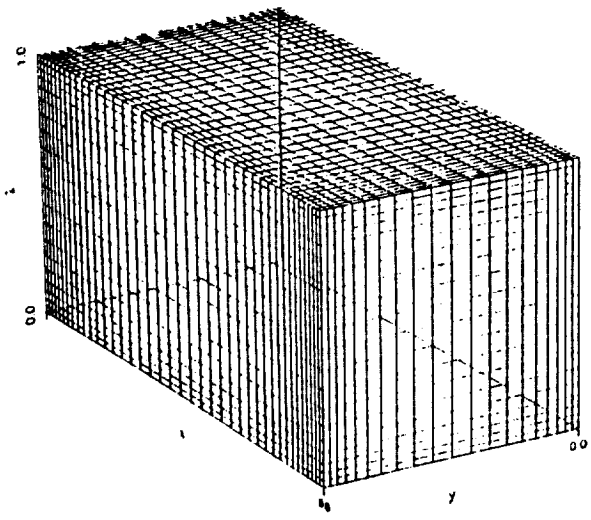

Figure 1. Computational grid and coordinate system

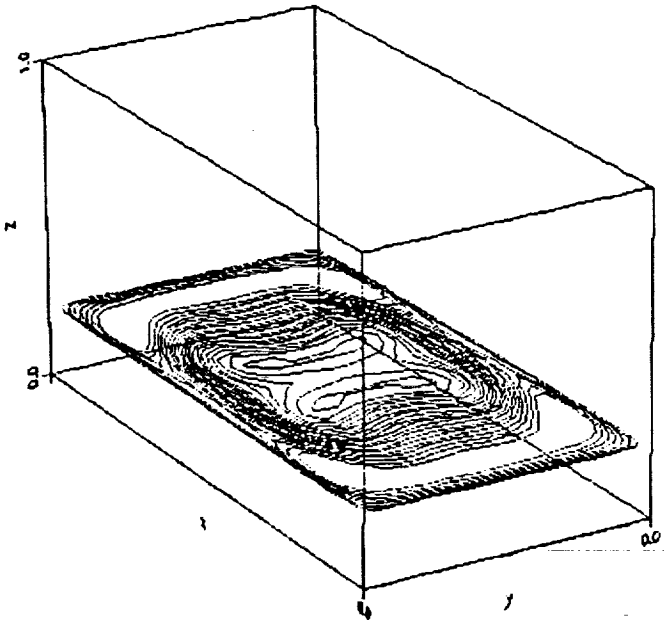

a

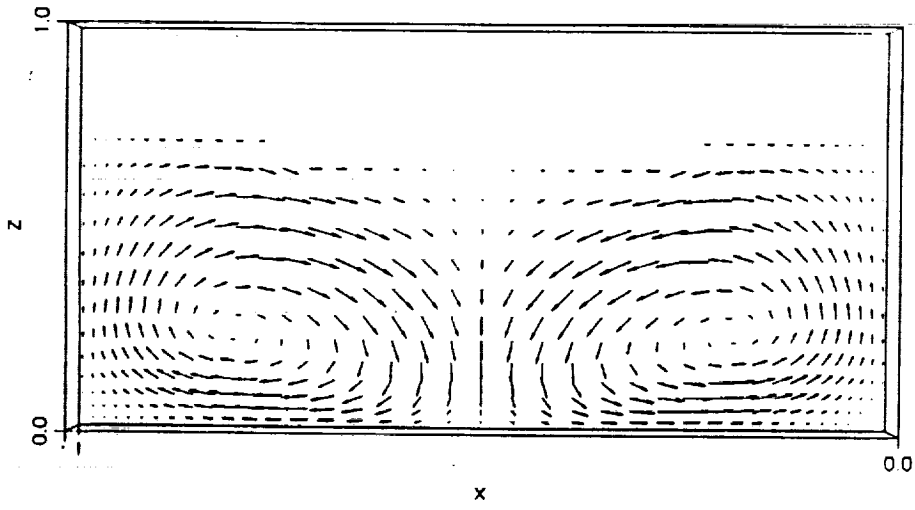

b

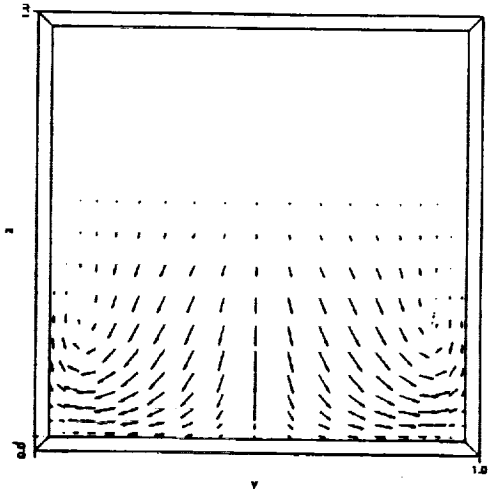

c

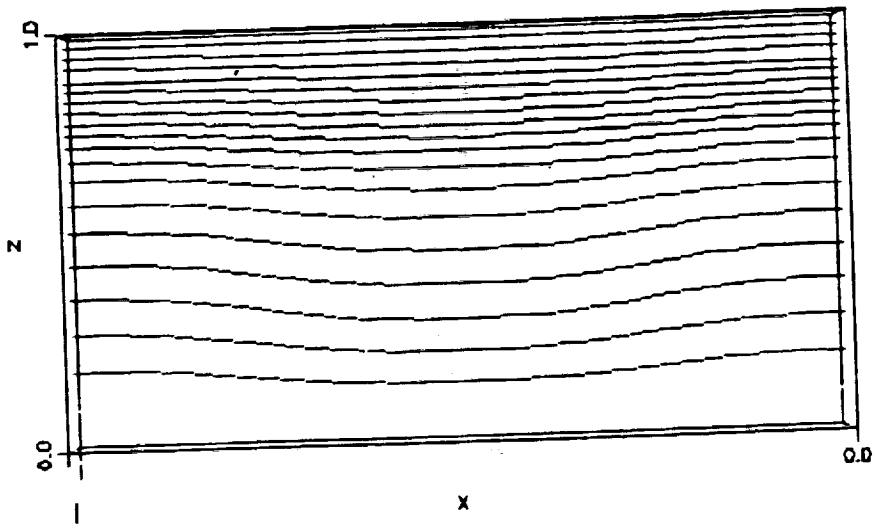

d

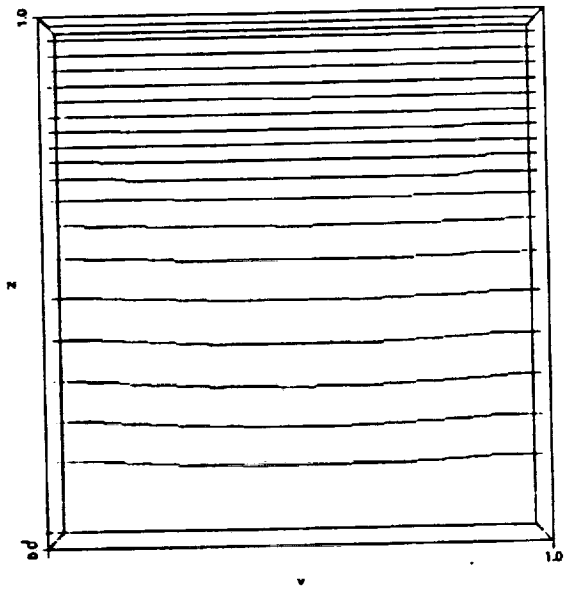

e

Figure 2. Solidification from the top: Ht = 0.
a) constant vertical velocity component contours at $z^* = 0.3$ horizontal plane; b) velocity vector field in vertical $y^* = 0.5$ mid-plane; c) velocity vector field in vertical $x^* = 0.5$ mid-plane; d) isotherms in vertical $y^* = 0.5$ mid-plane; e) isotherms in vertical $x^* = 0.5$ mid-plane.

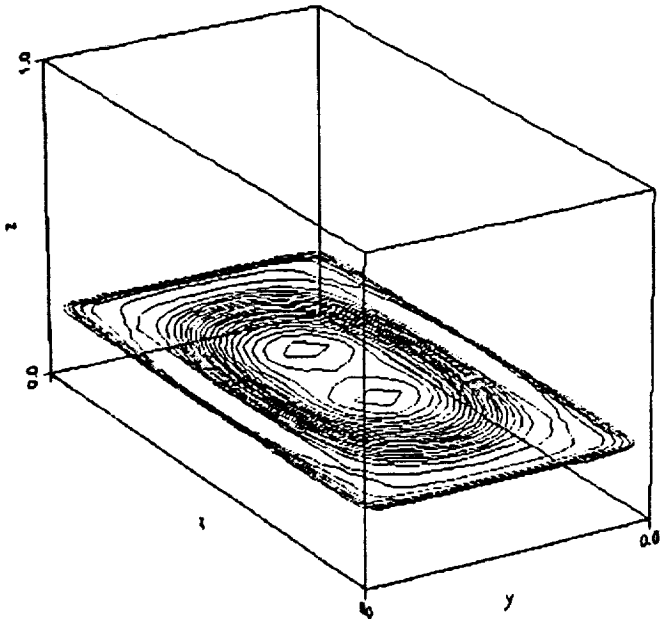

a

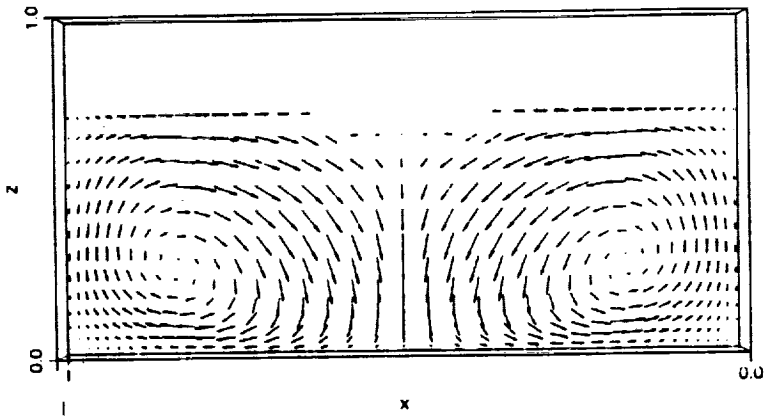

b

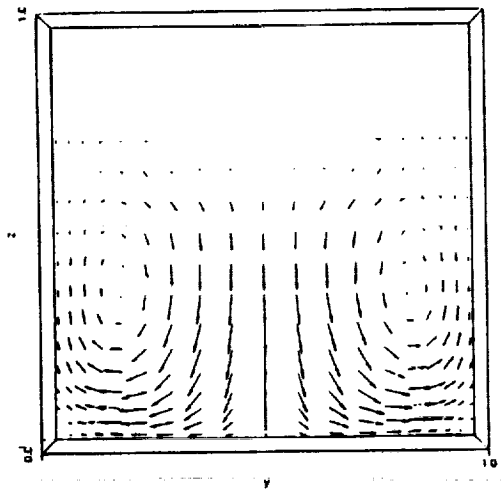

c

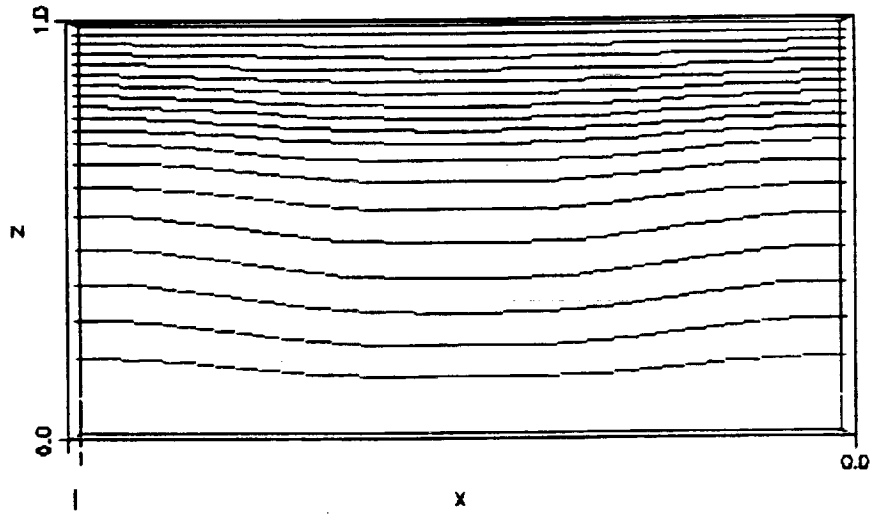

d

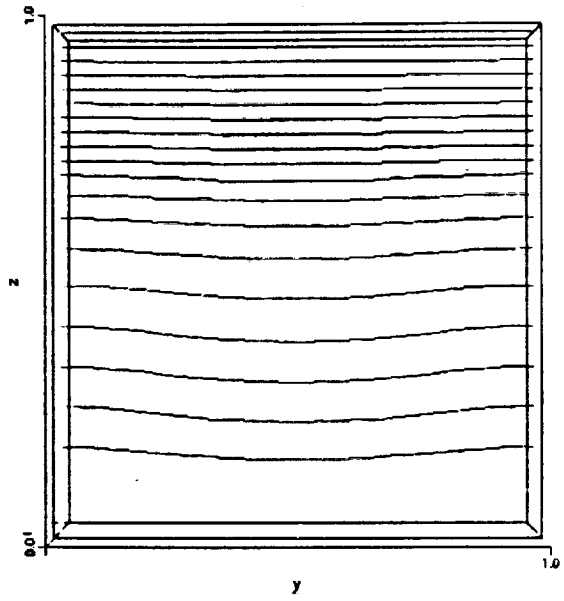

e

Figure 3. Solidification from the top: Ht = 20.
a) constant vertical velocity component contours at $z^* = 0.3$ horizontal plane; b) velocity vector field in vertical $y^* = 0.5$ mid-plane; c) velocity vector field in vertical $x^* = 0.5$ mid-plane; d) isotherms in vertical $y^* = 0.5$ mid-plane; e) isotherms in vertical $x^* = 0.5$ mid-plane.

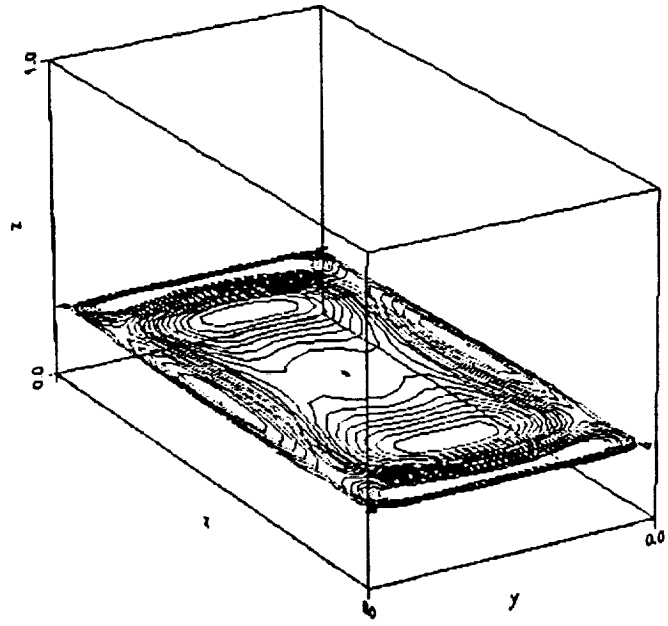

a

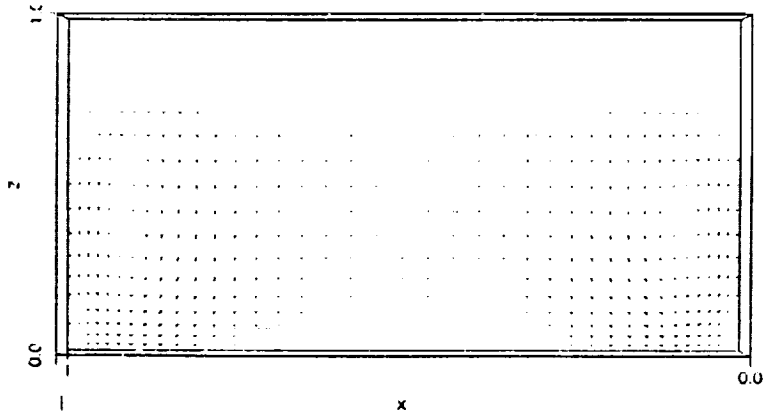

b

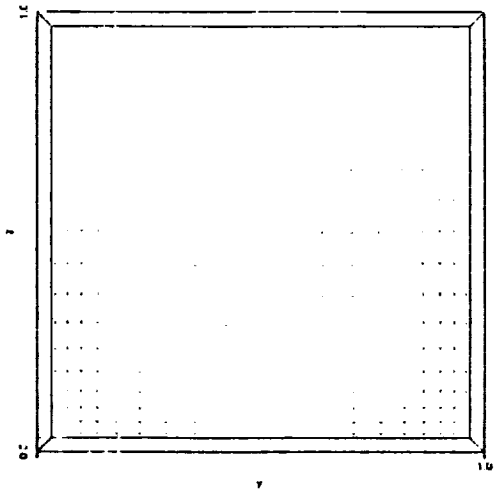

c

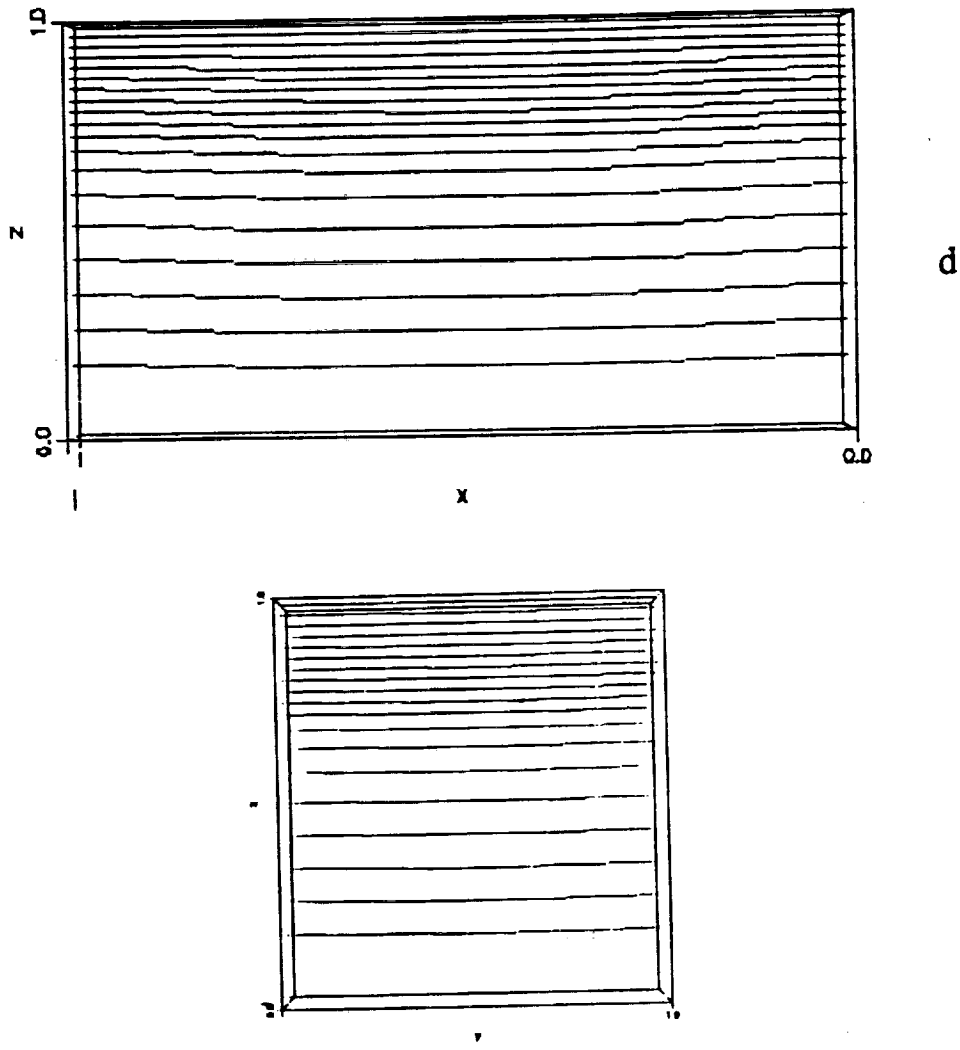

Figure 4. Solidification from the top: Ht = 60.
a) constant vertical velocity component contours at $z^* = 0.3$ horizontal plane; b) velocity vector field in vertical $y^* = 0.5$ mid-plane; c) velocity vector field in vertical $x^* = 0.5$ mid-plane; d) isotherms in vertical $y^* = 0.5$ mid-plane; e) isotherms in vertical $x^* = 0.5$ mid-plane.

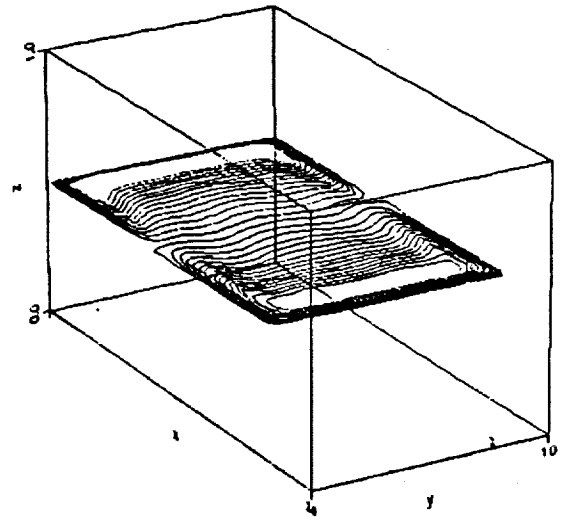

a

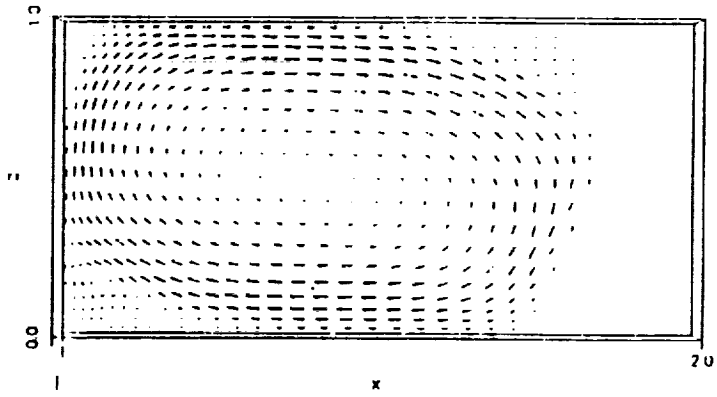

b

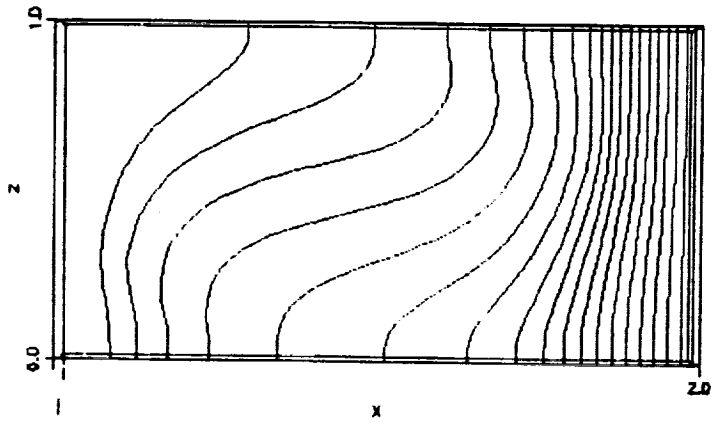

c

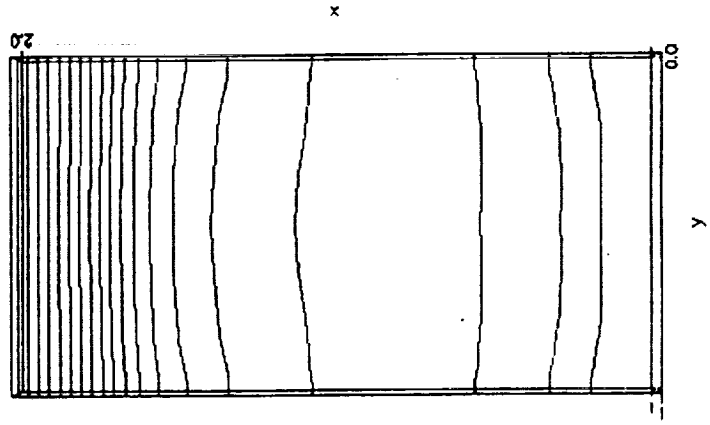

d

Figure 5. Solidification from the side: Ht = 0.
a) constant vertical velocity component contours at $z^* = 0.5$ horizontal mid-plane; b) velocity vector field in vertical $y^* = 0.5$ mid-plane; c) isotherms in vertical $y^* = 0.5$ mid-plane; d) isotherms in vertical $x^* = 0.5$ mid-plane.

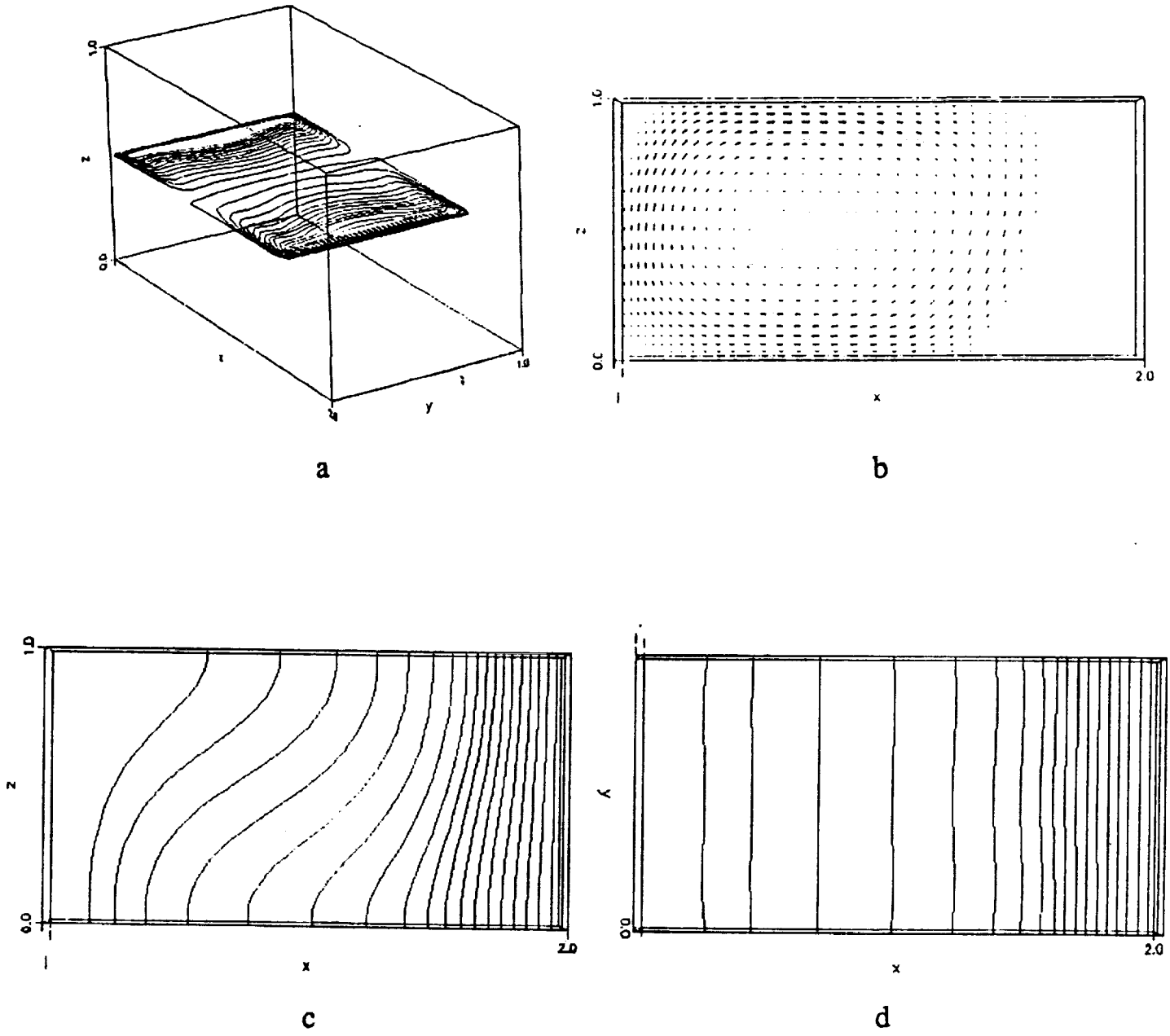

Figure 6. Solidification from the side: Ht = 30 applied vertically.
a) constant vertical velocity component contours at $z^* = 0.5$ horizontal mid-plane; b) velocity vector field in vertical $y^* = 0.5$ mid-plane; c) isotherms in vertical $y^* = 0.5$ mid-plane; d) isotherms in vertical $x^* = 0.5$ mid-plane.

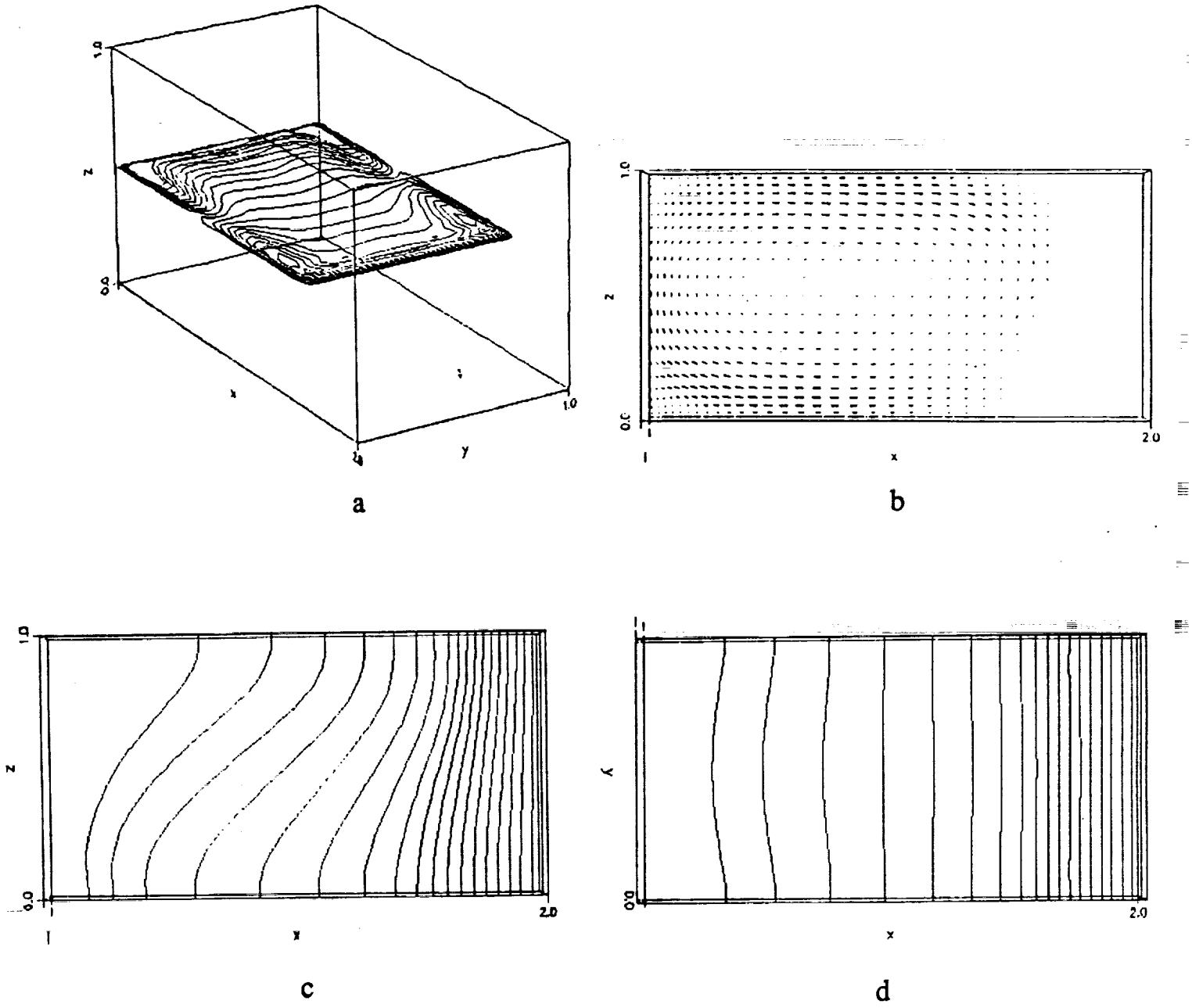

Figure 7. Solidification from the side: Ht = 30 applied in hot-to-cold direction.
a) constant vertical velocity component contours at $z^* = 0.5$ horizontal mid-plane; b) velocity vector field in vertical $y^* = 0.5$ mid-plane; c) isotherms in vertical $y^* = 0.5$ mid-plane; d) isotherms in vertical $x^* = 0.5$ mid-plane.

Session
Six

Analysis Techniques